THE JOURNAL OF BIOLOGICAL CHEMISTRY
Vol. 276, No. 14, Issue of April 6, pp. 11062–11071, 2001

Printed in U.S.A.

Entropic Stabilization of the Tryptophan Synthase α-Subunit from a Hyperthermophile, *Pyrococcus furiosus*

X-RAY ANALYSIS AND CALORIMETRY*

Received for publication, November 2, 2000, and in revised form, December 1, 2000
Published, JBC Papers in Press, December 14, 2000, DOI 10.1074/jbc.M009987200

Yuriko Yamagata‡, Kyoko Ogasahara§, Yusaku Hioki§, Soo Jae Lee§, Atsushi Nakagawa§, Haruki Nakamura§, Masami Ishida¶, Seiki Kuramitsu‖, and Katsuhide Yutani§**

From the ‡Graduate School of Pharmaceutical Sciences, and §Institute for Protein Research, Osaka University, Yamadaoka, Suita, Osaka 565-0871, Japan, the ¶Tokyo University of Fisheries, Konan Minato-ku, Tokyo 108-8477, Japan, and the ‖Graduate School of Sciences, Osaka University, Machikaneyama, Toyonaka, Osaka 560-0043, Japan

The structure of the tryptophan synthase α-subunit from *Pyrococcus furiosus* was determined by x-ray analysis at 2.0-Å resolution, and its stability was examined by differential scanning calorimetry. Although the structure of the tryptophan synthase $\alpha_2\beta_2$ complex from *Salmonella typhimurium* has been already determined, this is the first report of the structure of the α-subunit alone. The α-subunit from *P. furiosus* (*Pf*-α-subunit) lacked 12 and 6 residues at the N and C termini, respectively, and one residue each in two loop regions as compared with that from *S. typhimurium* (*St*-α-subunit), resulting in the absence of an N-terminal helix and the shortening of a C-terminal helix. The structure of the *Pf*-α-subunit was essentially similar to that of the *St*-α-subunit in the $\alpha_2\beta_2$ complex. The differences between both structures were discussed in connection with the higher stability of the *Pf*-α-subunit and the complex formation of the α- and β-subunits. Calorimetric results indicated that the *Pf*-α-subunit has extremely high thermostability and that its higher stability is caused by an entropic effect. On the basis of structural information of both proteins, we analyzed the contributions of each stabilization factor and could conclude that hydrophobic interactions in the protein interior do not contribute to the higher stability of the *Pf*-α-subunit. Rather, the increase in ion pairs, decrease in cavity volume, and entropic effects due to shortening of the polypeptide chain play important roles in extremely high stability in *Pf*-α-subunit.

Prokaryotic tryptophan synthase, which catalyzes the last processes in the biosynthesis of tryptophan, is a multienzyme $\alpha_2\beta_2$ complex composed of nonidentical α- and β-subunits. The separate α- and β_2-subunits catalyze inherent reactions termed α and β reactions, respectively. When the α- and β_2-subunits combine to form the $\alpha_2\beta_2$ complex, the enzymatic activity of each subunit is stimulated by 1 to 2 orders of magnitude (1). The $\alpha_2\beta_2$ complex has been studied as an excellent model system for seeking answers to important questions in protein-protein interaction, especially in multifunctional enzymes. In 1988 (2) the three-dimensional structure of the tryptophan synthase $\alpha_2\beta_2$ complex from *Salmonella typhimurium* was determined by x-ray analysis. However, the structure of the α- or β_2-subunit alone has not yet been determined. To elucidate the molecular basis of the mutual activation of the subunit interaction due to the formation of the $\alpha_2\beta_2$ complex, we need to know the structures of the α- or β_2-subunits alone as well as that of the complex. Although the crystallization of each subunit from *S. typhimurium* and *Escherichia coli* has been tried for many years (3), the report of the x-ray structure has not yet appeared. Recently, the structures of a number of proteins from hyperthermophiles have been successfully determined by x-ray analysis. This seems due to the facts that proteins from hyperthermophiles are unusually stable and more easily form better crystals. Therefore, the *trpA* and *trpB* genes, coding for tryptophan synthase, were cloned from *Pyrococcus furiosus* and their products were overexpressed in *E. coli*. The purified α-subunit from *P. furiosus* easily grew a suitable crystal for x-ray analysis, and the crystal structure could be determined at a resolution of 2.0 Å as described in this paper.

On the other hand, a fundamental understanding of the conformational stability of proteins still remains elusive. Proteins from hyperthermophiles should retain their native structures under extreme conditions, whereas the homologous proteins from mesophiles completely denature. Therefore, comparative studies of extremely thermostable proteins with their homologs might help us understand the stabilization mechanism of a general globular protein. Recently, structures and physicochemical properties of proteins from hyperthermophiles have been extensively studied. In several hyperthermophile proteins, an increased number of ion pairs and ion pair networks have been observed (4–13), which have been explained as the intrinsic changes for protein stability in hyperthermophiles. In the case of the tryptophan synthase α-subunit from *P. furiosus*, many ion pairs were also found. However, the effect of a surface salt bridge on the stability remains controversial even today; some reports have shown little contribution of a surface salt bridge to stability (14–19), whereas others have shown a favorable contribution (20–24). There are also reports on some hyperthermophile proteins without additional ion pairs (25–28). The conformation of general globular proteins is marginally maintained by the combination of many positive (such as hydrophobic interaction and hydrogen bond) and negative (such as entropic effect and steric hindrance) factors for stabilization (29). The enhanced stability of hyperthermophile proteins might originate from several attractive

* This work was supported in part by a grant-in-aid for special project research from the Ministry of Education, Science, and Culture of Japan (to K. Y.) and by the Structural Biology Sakabe Project (to K. Y., A. N., and Y. Y.). The costs of publication of this article were defrayed in part by the payment of page charges. This article must therefore be hereby marked "*advertisement*" in accordance with 18 U.S.C. Section 1734 solely to indicate this fact.

** To whom correspondence should be addressed: Institute for Protein Research, Osaka University, 3-2 Yamadaoka, Suita, Osaka 565-0871, Japan. Tel.: 81-6-6879-8615; Fax: 81-6-6879-8616; E-mail: yutani@protein.osaka-u.ac.jp.

forces (30). However, it still remains unclear what causes the dramatic stabilization of proteins from hyperthermophiles. Understanding the molecular origin for stabilization of hyperthermophile proteins provides valuable insights into the problems of protein stability, protein folding, and protein engineering.

In this paper, to elucidate the stabilization mechanism of a protein from a hyperthermophile, the stability of the α-subunit from *P. furiosus* (*Pf*-α-subunit)[1] was examined by differential scanning calorimetry (DSC) and its structure by x-ray crystallography. The DSC data indicated that the higher stability of this protein was not caused by an enthalpic factor as compared with homologous mesophile proteins. The stabilization mechanism of the *Pf*-α-subunit is discussed on thermodynamic grounds based on structural information from x-ray analysis.

EXPERIMENTAL PROCEDURES

Purification of the α-Subunit from P. furiosus—The α-subunit of tryptophan synthase from *P. furiosus* (*Pf*-α-subunit) was overexpressed in *E. coli* strain JM109/pα1974 containing only the *trpA* gene from *P. furiosus*.[2] The *E. coli* strain was routinely grown in 15 liters of LB medium supplemented with ampicillin of 100 mg/liter of culture medium. The production of the *Pf*-α-subunit was induced by addition of isopropyl-β-D(−)-thiogalactopyranoside at a concentration of 1 mM to the culture medium after 1-h incubation at 37 °C with shaking. Then the culture was continued for about 20 h at 37 °C with shaking.

Pelleted cells (wet weight of about 25 g) collected by centrifugation (5000 rpm for 10 min) were suspended in 100 ml of 20 mM potassium phosphate buffer (pH 7.0) containing 1 mM EDTA and 5 mM DTT. The cells were disrupted by sonication on ice for 5 min with cooling intervals for 10 min and repeating three times. The homogenized solution was heated in a water bath for 10 min at 75 °C (the temperature of the solution), under which the majority of the *E. coli* proteins precipitated, leaving the *Pf*-α-subunit in the soluble fraction. The resultant suspended solution was centrifuged at 15,000 rpm for 30 min at 4 °C to remove cell debris and denatured *E. coli* proteins. The supernatant solution was treated with ammonium sulfate of 40% saturation and centrifuged, and the precipitate was discarded. The *Pf*-α-subunit was precipitated by addition of ammonium sulfate at 90% saturation. The precipitate was dissolved in 50 ml of 25 mM potassium phosphate buffer (pH 7.0) with 1 mM EDTA and 5 mM DTT and dialyzed against the same buffer overnight at 4 °C.

The dialyzed sample was applied on a column (2.5 × 20 cm) of DEAE-Sephacel (Amersham Pharmacia Biotech): the enzyme was eluted with a linear gradient (25–200 mM) of potassium phosphate buffer (pH 7.0) containing 1 mM EDTA and 5 mM DTT. Active fractions of the eluted solutions were concentrated using an Amicon PM10 membrane filter. Next, the protein was separated by gel filtration (Superdex TM200 26/60, Amersham Pharmacia Biotech). The active fractions collected were finally purified by ion exchange chromatography (SP-Sepharose 26/16, Amersham Pharmacia Biotech) with a linear gradient of 25–100 mM phosphate buffer (pH 7.0) containing 1 mM EDTA and 5 mM DTT. The purified protein showed a single band on SDS-polyacrylamide gel electrophoresis.

Protein Concentration—The protein concentration was estimated from absorbance at 278.5 nm at pH 7.0, $OD_{1\%} = 6.92$, using a cell with a light path length of 1 cm. The value was determined based on a protein assay by the Lowry method using bovine serum albumin as a standard protein.

Differential Scanning Calorimetry—DSC was carried out with a differential scanning calorimeter, MicroCal VP-DSC (Northampton) at a scan rate of 1 K/min. Prior to the measurements, the protein solution was dialyzed against the buffer used. The dialyzed sample was filtered through a 0.22-μm pore size membrane and then degassed in vacuum. The buffers used were 20 mM glycine-HCl in the acidic region and 20 mM glycine-KOH in the alkaline region. The protein concentrations under measurement were 0.4–1.4 mg/ml. The DSC curves were analyzed by the Origin software from MicroCal (Northampton).

Crystallization and Data Collection—Crystals suitable for data collection were grown by the hanging drop vapor diffusion method at 10 °C from a reservoir solution containing 0.1 M MES-NaOH, pH 6.5, and 12% polyethylene glycol 20000. X-ray data from the native and mercury derivative crystals were collected at the beam line 18B of the Photon Factory, Tsukuba using a Weissenberg camera (32) at 293 K. The data set of the platinum derivative was collected on a Rigaku R-axis IV imaging plate using nickel-filtered double-mirror focused Cu-K_α radiation from a Rigaku RU-200. The native and derivative data were processed and integrated by DENZO and scaled by SCALEPACK (33). The space group is $C222_1$, and the unit cell dimensions are $a = 73.013$, $b = 78.997$, and $c = 170.964$ Å (see Table II below). There were two molecules in the asymmetric unit with a volume per unit of molecular weight of the protein of 2.30 Å^3/Da and a calculated solvent content of 53.4% (34).

Structure Determination and Refinement—Native, mercury, and platinum data sets were used for phase calculation by MIRAS (see Table II). The mercury position was identified in the difference Patterson map. Heavy atom sites in the platinum derivative were found in the difference Fourier maps calculated by using the phases from the first derivative with the program MLPHARE (35). The heavy atom parameters were refined, and the phases were calculated to 2.2 Å with the program SHARP (36). The initial MIR phases were improved by solvent flattening and noncrystallographic 2-fold symmetry averaging at the same resolution with the program SOLOMON (37). An initial model was built using the program O (38). Several cycles of rigid-body refinement, positional refinement, and simulated annealing were performed at 2.2-Å resolution with X-PLOR (39). The refinements were continued at 2.0 Å using CNS (40). Successive refinement with temperature factors and addition of solvents resulted in an R-value of 19.8% and an R_{free} of 24.9% for reflections in the resolution range 40–2.0 Å. R_{free} was calculated with 5% of the reflections. During refinements NCS restraints were enforced. The current model includes residues 1–166, 174–248 for molecule a and 1–169, 173–248 for molecule b, and 421 water molecules. Model geometry was analyzed with PROCHECK (41), and 96.4% of the nonglycine residues were in the most favorable region of the Ramachandran plot and 3.3% in the additionally allowed region. The final coordinates have been deposited in the Protein Data Bank (accession number 1GEQ).

Calculation of Electrostatic Interaction—The electrostatic free energy G_{el} of the protein-solvent system is generally described by a sum of the direct Coulombic energy and the dielectric shielding from the solvent due to the reaction field (42),

$$G_{el} = \frac{1}{2}\sum_{i\neq j}\frac{q_i q_j}{\epsilon_p|r_i - r_j|} + \frac{1}{2}\sum_i q_i \varphi^{react}(r_i) \quad \text{(Eq. 1)}$$

The potential energy $\varphi^{react}(r_i)$ due to the dielectric shielding at the ith charge position r_i, can be given as the difference between the electrostatic potentials $\varphi^{sol}(r_i)$ and $\varphi^{vac}(r_i)$, both of which were calculated by numerically solving the Poisson equations,

$$\Delta\epsilon(r)\Delta\varphi(r) = -4\pi\sum q_i\delta(r - r_i) \quad \text{(Eq. 2)}$$

assuming $\epsilon_p = 10$ and $\epsilon_p = \epsilon_s = 80$, respectively. Here, q_i is the ith charge and ϵ_p and ϵ_s are the dielectric constants $\epsilon(r)$ in the protein region and in the solvent region, respectively. ϵ_s in the solvent region was always assumed to be 80. The divergence of the electrostatic potential due to the self-Coulombic energy can be completely avoided, because the delta function in the right-hand side in eq. 2 is replaced by the smooth charge density in the actual numerical calculations (42).

In the continuum model for the native state, only the ionic charges were assumed as q_i to be located on both carboxyl oxygen atoms of the side chains of Asp and Glu, on the Nζ atoms of Lys, on the Cζ atoms of Arg, and on an N atom of the N terminus, respectively. When a strong ion pair is formed within 3 Å between the two heavy atoms, −e charge was assumed on one of the two carboxyl oxygen atoms of Asp or Glu, which is the closest to the positively charged residue, and +e charge was on Nη1, Nη2, or Nε, which is the closest to the negatively charged residue, in the case of Arg. Then, the above Poisson equations were numerically solved twice for the different ϵ_p values.

For the denatured state, the Coulombic term was calculated by using the root mean square distance $\langle r_{ij}^2\rangle^{1/2}$ between the ith and jth charges in the different residues as the distance between those charges. We evaluated the mean square distance between the corresponding Cα atoms for a simplified protein chain model, which was approximated by a Gaussian chain composed of only the connected Cα atoms, with the mean inter-Cα bond length 3.8 Å and the angle between the successive

[1] The abbreviations used are: *Pf*-α-subunit, tryptophan synthase α-subunit from *P. furiosus; Ec*-α-subunit, tryptophan synthase α-subunit from *E. coli*; *St*-α-subunit, tryptophan synthase α-subunit from *S. typhimurium*; DSC, differential scanning calorimetry; DTT, dithiothreitol; MES, 4-morpholineethanesulfonic acid; ASA, accessible surface area.

[2] M. Ishida, T. Oshima, and K. Yutani, manuscript in preparation.

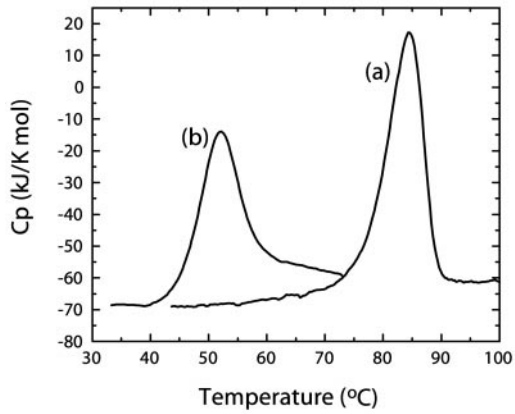

FIG. 1. **Typical excess heat capacity curves of tryptophan synthase α-subunits from *P. furiosus* and *E. coli* near pH 9.5 in 20 mM Gly-KOH buffer.** (*a*), *Pf*-α-subunit, at pH 9.60 and protein concentration of 0.40 mg/ml; (*b*), *Ec*-α-subunit, at pH 9.54, and protein concentration of 0.93 mg/ml.

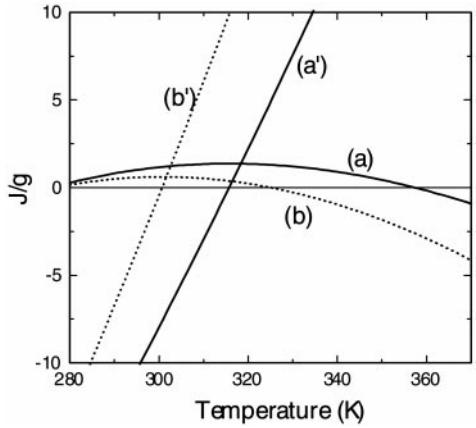

FIG. 3. **Specific Gibbs energy change (Δ*G*) and specific entropy change (*T*Δ*S*) upon denaturation of tryptophan synthase α-subunits from *P. furiosus* and *E. coli* as a function of temperature at pH 9.5.** *(a)* and *(a')* represent Δ*G* and *T*Δ*S* of *Pf*-α-subunit, respectively. *(b)* and *(b')* represent Δ*G* and *T*Δ*S* of *Ec*-α-subunit, respectively.

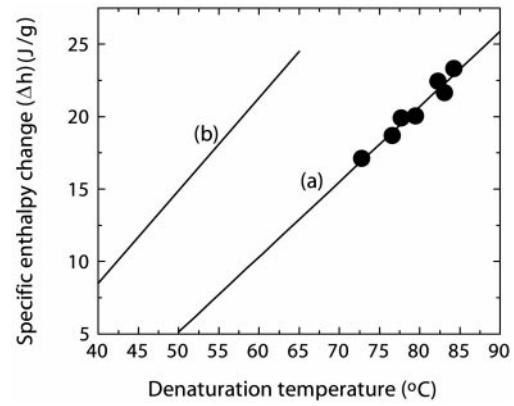

FIG. 2. **Specific enthalpy change upon denaturation for tryptophan synthase α-subunit from the *P. furiosus* as a function of denaturation temperature.** *Filled circles* represent each experimental point of *Pf*-α-subunit obtained at various pHs. *Line (a)* was given by a least-square fit to experimental points. *Line (b)* is a reported one for the *Ec*-α-subunit and the *St*-α-subunit (44).

three Cα atoms 106.3° (43). Adding the squared distances between the Cα atom and the charge position in each extended side chain for the *i*th and *j*th charges, respectively, r_{ij}^2 in the denatured state was estimated. As the value of $(\varphi^{sol}(r_i) - \varphi^{vac}(r_i))$ in the denatured state, the Poisson equations were solved for the models of the extended amino acid trimers, Ala-Xaa-Ala, where Xaa is Asp, Glu, Lys, or Arg. No charges were assumed on the N or C termini in the trimer models. The interaction term between the *i*th and *j*th charges in the reaction field calculation was neglected in the denatured states. A similar calculation was also performed for the N terminus using the extended Met-Ala model, assuming +e charge on the N atom of Met.

RESULTS

Thermal Stability of the α-Subunit of Tryptophan Synthase from P. furiosus—To examine the thermal stability of the *Pf*-α-subunit, DSC measurements were carried out at various pH values. Fig. 1 shows excess heat capacity curves of both the *Pf*-α-subunit and α-subunits from *E. coli* (*Ec*-α-subunit) near pH 9.5. The denaturation temperature of the *Pf*-α-subunit was about 33 °C higher than that of the *Ec*-α-subunit at the same conditions, indicating that the protein from a hyperthermophile has extremely high thermostability. In the acidic region from pH 3 to 4, the heat denaturation of the *Pf*-α-subunit was almost completely reversible, but the *Ec*-α-subunit was acid-denatured at room temperature. In Fig. 2 the specific enthalpy changes upon denaturation (Δ*h*, the enthalpy value per a gram of proteins) obtained from DSC curves of the *Pf*-α-subunit at various pH values are plotted against the denaturation temperature at each pH. *Line (a)* represents a least-square fit to the experimental points of the *Pf*-α-subunit. The slope corresponds to the specific heat capacity change of denaturation (Δc_p). The Δc_p value (0.52 J K^{-1} g^{-1}) of the *Pf*-α-subunit was slightly smaller than those of the *Ec*-α-subunit and the α-subunit from *S. typhimurium* (*St*-α-subunit), which are similar to each other (0.64 J K^{-1} g^{-1} from the slope of *line 2* in Sugisaki *et al.* (44)). The figure indicates that Δ*h* values of the *Pf*-α-subunit were considerably lower than those of mesophile proteins at each temperature shown in the figure: for example, Δ*h* was 10.3 J/g and 21.4 J/g for those from the *Pf*-α-subunit and mesophile proteins, respectively, at 60 °C. The thermodynamic parameters for heat denaturation as a function of temperature can be calculated using the following equations,

$$\Delta h(T) = \Delta h(T_d) - \Delta c_p(T_d - T) \quad \text{(Eq. 3)}$$

$$\Delta s(T) = \Delta h(T_d)/T_d - \Delta c_p \ln(T_d/T) \quad \text{(Eq. 4)}$$

$$\Delta g(T) = \Delta h(T) - T\Delta s(T) \quad \text{(Eq. 5)}$$

assuming that Δc_p does not depend on temperature (45). The temperature functions of Δ*g* for the *Pf*-α-subunit and the *Ec*-α-subunits at pH 9.5 obtained from eq. 5 are shown in Fig. 3, indicating that the *Pf*-α-subunit is more stable than the *Ec*-α-subunit under all the temperatures shown. The difference in Δ*g* was remarkable at higher temperatures. Because the denaturation enthalpies of the *Pf*-α-subunit under all the temperatures as shown in Fig. 2 are lower than those of the *Ec*-α-subunit, the increase in Δ*g* of *Pf*-α-subunit comes from the decrease in Δs as shown in Fig. 3.

Amino Acid Compositions and Overall Structure of the α-Subunit from P. furiosus—The *Pf*-α-subunit consists of 248 residues,[2] but the *St*-α-subunit has 268 (2). Table I shows the amino acid compositions of both α-subunits. Hydrophobic residues of the *Pf*-α-subunit were reduced from 157 (58.6%) to 133 (53.6%) as compared with those of the *St*-α-subunit: especially, Ala was 40 (14.9%) to 22 (8.9%). On the other hand, the hydrophilic residues were increased from 64 (23.9%) to 80 (32.3%): especially, Lys was 8 (3.0%) to 20 (8.1%). Jaenicke *et al.* (46) have reported that the ranking of the five most frequent amino acid exchanges from mesophiles to hyperthermophiles is seen to be Lys → Arg, Ser → Ala, Gly → Ala, Ser → Thr, and Ile → Val. In the case of the *Pf*-α-subunit, however, Lys was remarkably increased and Ala decreased.

For the structure determination of the *Pf*-α-subunit, the

TABLE I
Comparison of amino acid compositions of tryptophan synthase α-subunits from P. furiosus and S. typhimurium

Residues	α-Subunit from *P. furiosus*[a]		α-Subunit from *S. typhimurium*[a]	
	Residue number	% of residue per total number	Residue number	% of residue per total number
		%		%
Hydrophobic	133	53.63	157	58.58
Gly	21	8.47	20	7.46
Ala	22	8.87	40	14.93
Val	21	8.47	17	6.34
Leu	25	10.08	28	10.45
Ile	17	6.85	18	6.72
Met	3	1.21	5	1.87
Phe	13	5.24	12	4.48
Trp	1	0.40	0	0.00
Pro	10	4.03	17	6.34
Neutral	35	14.11	47	17.54
Ser	11	4.44	16	5.97
Thr	14	5.65	7	2.61
Asn	7	2.82	11	4.10
Gln	2	0.81	10	3.73
Cys	1	0.40	3	1.12
Hydrophilic	80	32.26	64	23.88
Asp	12	4.84	13	4.85
Glu	20	8.06	16	5.97
Lys	20	8.06	8	2.99
His	4	1.61	5	1.87
Arg	15	6.05	15	5.60
Tyr	9	3.63	7	2.61
Total number	248		268	

[a] Amino acid compositions are taken from Ishida *et al.*[2] and Hyde *et al.* (2).

TABLE II
Data collection, phasing, and refinement statistics of tryptophan synthase α-subunit from P. furiosus

Data set	Native	Hg	Pt
Data collection			
Wavelength (Å)	1.0000	1.0000	1.5418
Resolution range (Å)	40.0–2.0	40.0–2.2	40.0–3.2
Unique observations	31,934	23,394	8,090
Total observations	90,544	83,106	24,473
Completeness (%)			
Overall (final shell)	94.2 (93.9)	91.1 (93.9)	95.9 (74.8)
R_{merge}[a]			
Overall (final shell)	0.035 (0.167)	0.053 (0.216)	0.092 (0.198)
MIRAS phasing			
R_{cullis} (acentric/centric)[b]		0.75/0.81	0.92/0.91
R_{cullis}–anomalous		0.77	
Phasing power (acentric/centric)[c]		1.73/1.11	1.06/1.06
Phasing power–anomalous		1.62	
Figure of merit		0.31	
Refinement statistics			
Resolution range (Å)	40.0–2.0		
R-factor (%)[d]	19.8		
R_{free} (%)	24.9		
Root mean square deviations from ideality			
Bond distances (Å)	0.006		
Bond angles (°)	1.2		

[a] $R_{merge} = 100 \times \Sigma|I_{h,i} - \langle I_h\rangle|/\Sigma I_{hi}$. $I_{h,i}$ are individual values, and $\langle I_h\rangle$ is the mean value of the intensity of reflection h.
[b] $R_{cullis} = \langle$phase-integrated lack of closure$\rangle/\langle|$Fph-Fp$|\rangle$.
[c] Phasing power = $\langle[|Fh(\text{cal})|/$pase-integrated lack of closure$]\rangle$.
[d] *R*-factor = $\Sigma||F_o| - |F_c||/\Sigma|F_o|$.

molecular replacement method using the structure of the α-subunit in the $\alpha_2\beta_2$ complex of tryptophan synthase from *S. typhimurium* (2) as a search model, was tried using AMoRe (47) or X-PLOR (39), because the sequence identity of both proteins was 31.5%. But all attempts to refine the solution failed. Therefore, the structure of the *Pf*-α-subunit was solved by the method of multiple isomorphous replacement using two derivatives with K_2PtCl_4 and CH_3HgCl (Table II). It was found that the *Pf*-α-subunit adopts an 8-fold α/β barrel fold, first observed in a triose-phosphate isomerase barrel (48), similar to that of the *St*-α-subunit (2), as shown in Figs. 4 and 6. The helices and strands corresponding to canonical α/β barrel elements have been numbered consecutively 1 to 8. In the structure of the *St*-α-subunit, an extra helical segment, designated helix 0, precedes the first strand and acts as a cap in the bottom of the barrel (2). However, in the *Pf*-α-subunit the helix 0 was not observed because of the missing 12 residues in the N-terminal region as compared with the *St*-α-subunit. Six residues in the C-terminal helix 8 were also deleted in the *Pf*-α-subunit. Fig. 5 shows the secondary structure-based sequence alignment using the secondary structure elements assigned using DSSP (49). This alignment also suggests that another two residues

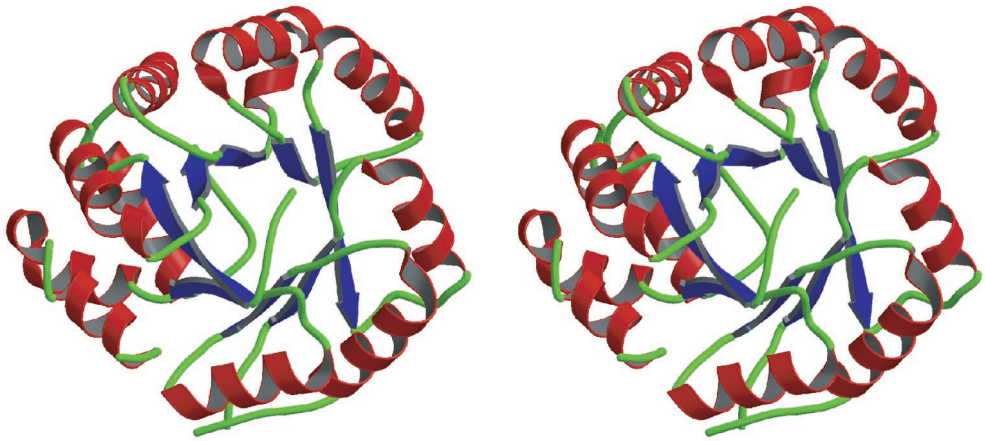

FIG. 4. **Schematic stereo view of the α-subunit of tryptophan synthase from *P. furiosus*.** Protein figures were prepared using the programs of MOLSCRIPT (76) and Raster3D (31).

```
  Helix-0          Strand-1          Helix-1          Strand-2          Helix-2'
1        10        20        30        40        50        60        70
MERYENLFAQ LNDRREGAFV PFVTLGDPGI EQSLKIIDTL IDAGADALEL GVPFSDPLAD GPTIQNANLR
 HHHHHHHHH HHHTT  EEE EEEETTSS H HHHHHHHHHH HHTT SSEEE E   S  TT   HHHHHHHHH
               TTEEE EEEETTSS H HHHHHHHHHH  GGGBS EEE E   S  TTS  HHHHHHHHH
            MFKDGSLI PYLTAGDPDK QSTLNFLLAL -DEYAGAIEL GIPFSDPIAD GKTIQESHYR
            1        10        20        30        40        50

         Helix-2           Strand-3          Helix-3          Strand-4
        80        90        100       110       120       130       140
AFAAGVTPAQ CFEMLALIRE KHPTIPIGLL MYANLVFNNG IDAFYARCEQ VGVDSVLVAD VPVEESAPFR
HHHHT  HHH HHHHHHHHHH H SSS EEEE E HHHHHTT  HHHHHHHHHH HT  EEEETT   GGG HHHH
HHHTT  HHH HHHHHHHHHT T     EEEE E HHHHHHH  HHHHHHHHHH HT  EEEETT   GGGHHHHH
ALKNGFKLRE AFWIVKEFRR HSST-PIVLM TYYNPIYRAG VRNFLAEAKA SGVDGILVVD LPVFHAKEFT
 60        70        80        90        100       110       120

Helix-4  Strand-5     Helix-5   Strand-6                  Helix-6   Strand-7
       150       160       170       180       190       200       210
QAALRHNIAP IFICPPNADD DLLRQVASYG RGYTYLLSRS GVTGAENRGA LPLHHLIEKL KEYHAAPALQ
HHHHHTT EE EEEE TT  H HHHHHHHHH   S EEE ??? ????????    HHHHHHHH HHHT   EEE
HHHHHTT EE EEEE TT  H HHHHHHHHH  SSEEEEE SS    ???     HHHHHHHHHH HHH SS EEE
EIAREEGIKT VFLAAPNTPD ERLKVIDDMT TGFVYLVSLY GTTGAREEIP KTAYDLLRRA KRICRNKVAV
 130       140       150       160       170       180       190

      Helix-7    Strand-8   Helix-8'       Helix-8
      220       230       240       250       260      268
GFGISSPEQV SAAVRAGAAG AISGSAIVKI IEKNLASPKQ MLAELRSFVS AMKAASRA
 TT  SHHHH HHHHHHT SE EEE SHHHHH HHHTTT HHH HHHHHHHHHH HHHHHTT?
ES   SHHHH HHHHHTT SE EEE HHHHHH HHHHGGG HH HHHHHHHHHT T
GFGVSKREHV VSLLKEGANG VVVGSALVKI IGEKGREATE FLKKKVEELL GI
 200       210       220       230       240      248
```

FIG. 5. **Sequence alignments with secondary structures of α-subunits of tryptophan synthase from *P. furiosus* and *S. typhimurium*.** The *first line* represents the alias of secondary segments named by Hyde *et al.* (2). The *second* and *seventh lines* represent the residual numbers of the *St*-α-subunit and the *Pf*-α-subunit, respectively. The *third* and *sixth lines* represent amino acid sequences of *St*-α-subunit and *Pf*-α-subunit, respectively. The *fourth* and *fifth lines* represent secondary structural elements of *St*-α-subunit (1BKS) and *Pf*-α-subunit, respectively, judged from the secondary structure definition as established by DSSP (29). *H*, *E*, *B*, *G*, *T*, and *S* in the secondary structure elements represent α-helix, β-strand, β-bridge, 3-helix, turn, and bend, respectively. The residual names with *underlines* in the *third line* represent hydrogen-bonding residues in the *St*-α-subunit with the β-subunit. The residual names with *underlines* in *sixth line* represent residues in the *Pf*-α-subunit whose Cα atoms are deviated more than 2.5 Å as compared with those in the *St*-α-subunit (see Fig. 7).

corresponding to positions 41 and 95 in the *St*-α-subunit were deleted in the *Pf*-α-subunit. These deletions in the *Pf*-α-subunit might cause the decrease in entropy in the denatured state as compared with those from the mesophiles, resulting in stabilization of a protein conformation, as described under "Discussion."

Structural Comparison of Pf-α-subunit and St-α-subunit—The structures of the *Pf*-α-subunit and *St*-α-subunit (1BKS) could be superimposed with the root mean square deviation of 2.82 Å between 234 equivalent Cα atoms in both subunits (Fig. 6*a*). The seven remarkable deviations are found in Fig. 7. The three big deviations are indicated by *peaks I*, *VI*, and *VII* in Fig. 7. The deviation of *peak I* is caused by 12 missing residues in the N-terminal (the deletion of helix 0), where the bottom of the barrel is capped by a short loop in the place of helix 0 in *St*-α-subunit as shown in Fig. 6. *Peaks VI* and *VII* correspond to helices 6 and 8, respectively. The deviation at helix 8 (*peak VII*) is caused by missing six residues in the C terminus, resulting in a shorter helix with 11 residues from a long helix (18 residues) of the *St*-α-subunit. Residues 178–189 in a loop between strand 6 and helix 6 of the *St*-α-subunit are highly mobile, thus the positions are not determined due to weak electron density. This loop plays an important role in the intersubunit communication for enzymatic functions (50). In the case of the *Pf*-α-subunit, only three residues (170–172) could not be determined in contrast to 12 corresponding residues (164–175) of the *St*-α-subunit, indicating that the number of the mobile residues in the *Pf*-α-subunit was remarkably reduced. When the *St*-α-subunit in the $\alpha_2\beta_2$ form binds with the substrate inhibitors of the α-subunit, indole-3-propanol phosphate (50, 51) and 5-fluoroindole propanol phosphate (52), the disordered residues in their complexes have been reported to be reduced by two (190–191) and six (188–193) from 12 residues (178–189), respectively. These results indicate that the ligand binding induces confor-

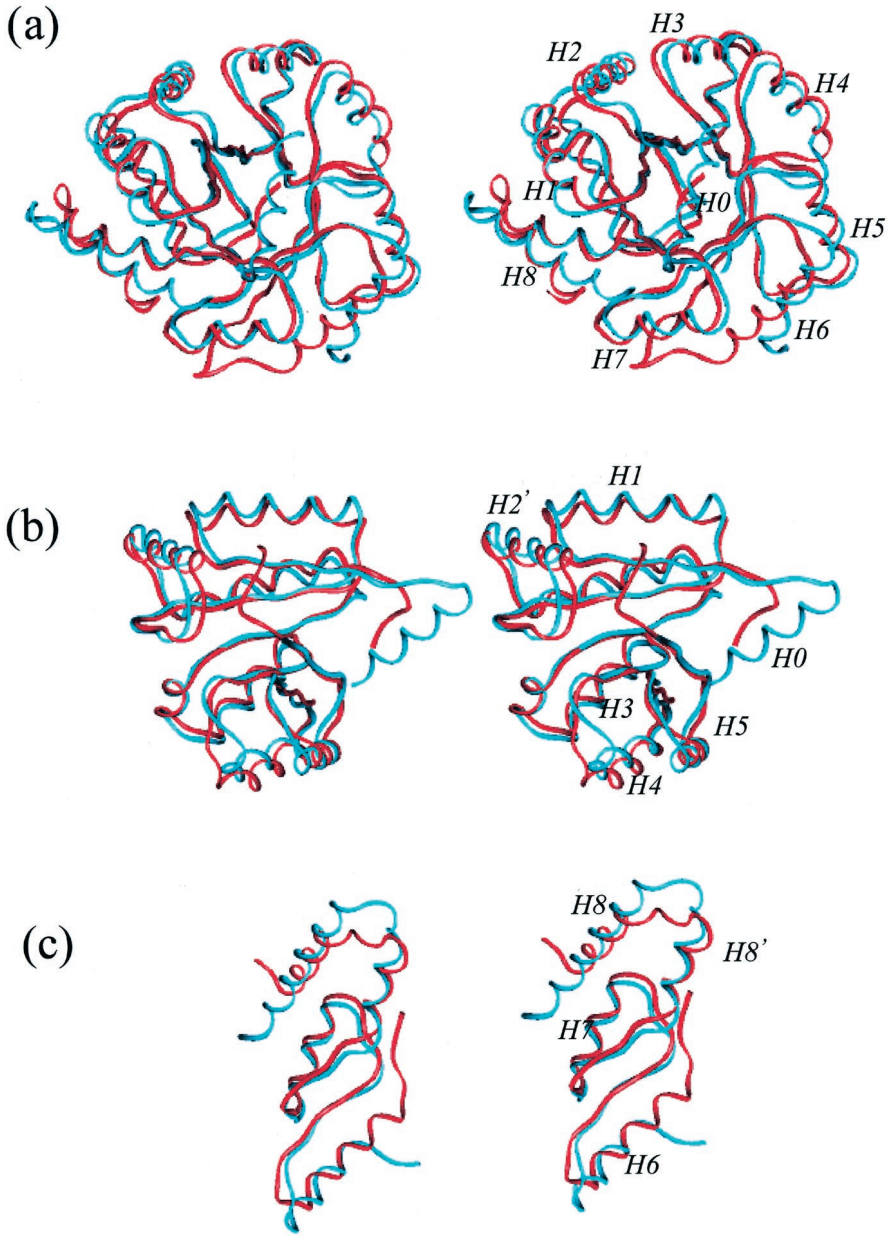

FIG. 6. **Schematic stereo view of the α-subunits of tryptophan synthase from *P. furiosus* and from *S. typhimurium* superimposed.** *Red* and *blue* represent the *Pf*-α-subunit and the *St*-α-subunit (1BKS), respectively. *H0* through *H8* represents helices 0 through 8 in the *St*-α-subunit, respectively. *(a)* represents the whole structures of both α-subunits. *(b)* and *(c)* represent stereo drawings of the main chains in the N- and C-terminal regions of tryptophan synthase α-subunits superimposed, respectively.

mational changes to less mobile forms. On the other hand the structure of the corresponding loop region of the *Pf*-α-subunit was remarkably different from that of the *St*-α-subunit with inhibitors (Fig. 6). This suggests that the loop region of the *Pf*-α-subunit might drastically change the conformation when the substrate (or inhibitor) binds to the protein.

Peaks II and *IV* in Fig. 7 are close to each residue corresponding to positions 41 and 95, respectively, in the *St*-α-subunit, which were deleted in the *Pf*-α-subunit. *Peak III* corresponds to helix 2′. In the case of the *St*-α-subunit a prominent deviation from the canonical triose-phosphate isomerase barrel is an insertion of 26 residues (positions 53–78) between strand 2 and helix 2. These residues, including helix 2′, are highly conserved in α-subunits among many species. Two catalytic residues (Glu^{49} and Asp^{60}) in the *St*-α-subunit are involved in or near the insertion region. The corresponding residues, Glu^{36} and Asp^{47}, in the *Pf*-α-subunit were also found at coordinates similar to those from the mesophile protein. Helix 2′ might be important in connection with enzyme function, although catalytic residues are not involved. In the region of *peak V* in the *St*-α-subunit, there are hydrogen-bonding residues (Val^{133}, Glu^{134}, and Glu^{135}) interacting with the β-subunit (Fig. 5), which are important residues in the complex formation (53). The deviations of the *peaks I*, *II*, *IV*, and *VII* were caused by the deletion of residues, but other peaks of deviations (*III*, *V*, and *VI*) were related to enzymatic function, suggesting that the conformation of these portions might be affected when the α-subunit forms the complex with the β_2-subunit.

High resolution structures of proteins from hyperthermophiles have shown that the number of ion pairs in most of the hyperthermophile proteins is higher than in mesophile counterparts (4–13), although additional ion pairs were not observed in some hyperthermophile proteins (25–28). Table III lists the ion pairs formed within 4 Å for the *Pf*-α-subunit and *St*-α-subunit. The number (0.05) of ion pairs per a residue for the *Pf*-α-subunit is relatively higher than that (0.02) for the *St*-α-subunit but is comparable to that (0.04) of the average number of mesophile proteins (54). In the *Pf*-α-subunit, 24 residues are involved in the formation of 13 ion pairs: five ion pairs for nine residues in the *St*-α-subunit. Only one ion pair, Arg^{57}-Asp^{15}, in the *Pf*-α-subunit is conserved in the *St*-α-subunit (Arg^{70}-Asp^{27}). Ion pairs in the *Pf*-α-subunit form between

the following structural segments: five intra-helical, three inter-helical, two between helix and loop, one between helix and β-strand, one between β-strands, and one between β-strand and loop (Table III).

The volume of the cavities in the subunits of glutamate dehydrogenase from three different species decreases significantly with increasing thermal stability of the enzymes (9). For two α-subunits of tryptophan synthase, the cavity volume was determined by attempting to insert a probe sphere of 1.4-Å radius (assuming a water molecule) (55). In the case of the *Pf*-α-subunit, seven cavities were found and the total volume was 226.8 $Å^3$; in the *St*-α-subunit eight cavities were found with 318.1 $Å^3$ volume (Table IV). The energy term of ΔG due to changes in the cavity size can be expressed in terms of the cavity volume (100–140 J mol^{-1} $Å^{-3}$) (56). Using this parameter (120 J mol^{-1} $Å^{-3}$) the increment in stabilization of the *Pf*-α-subunit due to the decrease in cavity volume could be calculated to be 11.0 kJ/mol (Table IV), as compared with that of the *St*-α-subunit.

Because the *B*-factor in x-ray analysis can correlate with the flexibility of atoms, *B*-factors averaged for the main-chain atoms of the *Pf*-α-subunit were examined along with those of the *St*-α-subunit. Both data were collected at room temperatures (293–300 K). The difference in *B*-factors between both proteins (Fig. 8) shows that two parts of the *Pf*-α-subunit, corresponding to *peaks I* and *II* in Fig. 8, are more mobile than those of the *St*-α-subunit. The residues of *peaks I* and *II* are Tyr^{93} and Phe^{120}, respectively. The corresponding residues in the *St*-α-subunit are Phe^{107} and Glu^{134}, which are the residues (or neighbor residues) hydrogen bonding with the β_2-subunit in the $\alpha_2\beta_2$ complex. This suggests that these residues (Tyr^{93} and Phe^{120}) in the *Pf*-α-subunit might become less flexible when the *Pf*-α-subunit associates with the β_2-subunit. The B-factor values in other parts of the *Pf*-α-subunit were relatively lower than those of the *St*-α-subunit. This may be due to enhanced thermal stability of proteins from hyperthermophiles in the standard state at 25 °C, caused by enhanced conformational rigidity in their folded native state (30).

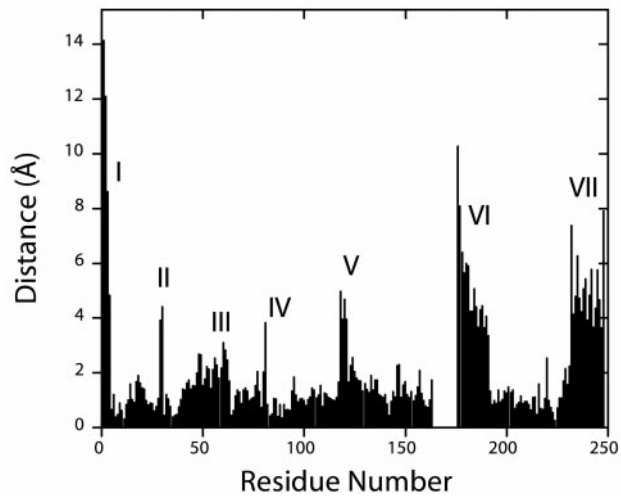

FIG. 7. **Root mean square deviations (Å) of Cα atoms between the *Pf*-α-subunit and the *St*-α-subunit after a least squares fit of corresponding Cα atoms.** *Peaks I* through *VII* represent only a discrimination peak of large differences. Residual numbers are for the *Pf*-α-subunit.

TABLE III
Ion pairs (salt bridges) in tryptophan synthase α-subunits from P. furiosus and S. typhimurium within 4 Å

No.	Positively charged side chain	Accessibility	Negatively charged side chain	Accessibility	Location	Distance
		%		%		Å
(A) *Pf*-α-subunit						
1	Arg-57:Nε	0	Asp-15:Oδ2	2.4	H2-S1	2.93
	Arg-57:NH2	0.3	Asp-15:Oδ1	0.1	H2-S1	2.96
	Arg-57:NH2	0.3	Asp-15:Oδ2	2.4	H2-S1	3.72
2	Arg-66:NH2	25.8	Glu-103:Oε2	18.0	L-H3′	3.02
3	Arg-76:NH2	0.5	Asp-110:Oδ1	0	H2′-L	2.60
	Arg-76:NH2	0.5	Asp-110:Oδ2	81.3	H2′-L	3.73
4	Arg-77:NH2	59.8	Glu-74:Oε1	35.9	H2′-H2′	3.49
5	Arg-98:Nε	37.2	Glu-132:Oε2	35.8	H3′-H4	2.86
	Arg-98:NH2	19.3	Glu-132:Oε2	35.8	H3′-H4	3.34
6	Arg-98:NH1	55.9	Glu-131:Oε2	9.8	H3′-H4	3.46
	Arg-98:NH2	19.3	Glu-131:Oε2	9.8	H3′-H4	2.54
7	Arg-184:NH1	43.0	Asp-181:Oδ2	40.7	H6-H6	2.57
	Arg-184:NH2	48.0	Asp-181:Oδ2	40.7	H6-H6	3.25
8	Arg-185:NH1	10.5	Asp-181:Oδ1	43.5	H6-H6	2.75
9	Arg-188:NH1	19.6	Asp-146:Oδ2	55.4	H6-H5	3.82
	Arg-188:NH2	33.2	Asp-146:Oδ1	2.8	H6-H5	3.97
	Arg-188:NH2	33.2	Asp-146:Oδ2	55.4	H6-H5	2.76
10	Arg-232:NH1	56.0	Asp-17:Oδ2	15.0	L-S1	2.53
	Arg-232:NH1	56.0	Asp-17:Oδ1	0.2	L-S1	3.68
	Arg-232:NH2	68.6	Asp-17:Oδ1	0.2	L-S1	3.99
11	Lys-193:Nζ	25.6	Asp-4:Oδ2	0.3	S7-S1	2.65
12	Lys-225:Nζ	85.7	Glu-229:Oε2	27.2	H8′-H8′	3.90
13	Lys-241:Nζ	28.7	Glu-244:Oε1	81.3	H8′-H8′	3.79
	Lys-241:Nζ	28.7	Glu-244:Oε2	42.0	H8′-H8′	3.47
(B) *St*-α-subunit						
1	Arg-3:NH1	25.5	Glu-2:Oε2	67.7	H0-H0	3.82
2	Arg-14:NH2	20.2	Glu-16:Oε2	1.5	L-H0	3.04
3	Arg-70:NH2	0	Asp-27:Oδ2	0.1	H2′-L	2.86
	Arg-70:NH2	0	Asp-27:Oδ1	0	H2′-L	3.18
4	His-92:Nε2	0	Asp-38:Oδ1	1.4	L-H1	2.66
5	Lys-91:Nζ	26.8	Asp-38:Oδ1	1.4	L-H1	3.98
	Lys-91:Nζ	26.8	Asp-38:Oδ2	38.2	L-H1	3.23

TABLE IV

Estimate of the difference in stability between α-subunits from P. furiosus and S. typhimurium on the basis of structural information

ΔG_{HP}, ΔG_{CAV}, ΔG_{ENT} ($= -T\Delta S$), and ΔG_{E1} represent ΔG values due to hydrophobic interaction, cavity volume, entropic effect, and electrostatic interaction, respectively.

	Pf-α-subunit	*St*-α-subunit	Δ(= *Pf* − *St*)
ASA value in N state			
C/S atoms	5,600 Å^2	6,097 Å^2	−497 Å^2
N/O atoms	5,515 Å^2	5,150 Å^2	365 Å^2
ASA value in D state			
C/S atoms	22,049 Å^2	23,015 Å^2	−966 Å^2
N/O atoms	12,468 Å^2	12,364 Å^2	104 Å^2
Difference of ASA values (D–N)			
C/S atoms	16,449 Å^2	16,918 Å^2	−469 Å^2
N/O atoms	6,953 Å^2	7,214 Å^2	−261 Å^2
ΔG_{HP}	2,837.3 kJ/mol	2,917.1 kJ/mol	−79.8 kJ/mol
Cavity Vol. (probe 1.4 Å)	226.75 Å^3	318.07 Å^3	−91.32 Å^3
ΔG_{CAV}	−27.2 kJ/mol	−38.2 kJ/mol	11.0 kJ/mol
Total number of residues	248	268	−20
ΔG_{ENT} at 25 °C			51.2 kJ/mol
ΔG_{ENT} at 60 °C			57.2 kJ/mol
Electrostatic energy (1)			
ΔG_{E1}	80.4 kJ/mol	37.7 kJ/mol	42.7 kJ/mol
Electrostatic energy (2)			
Native state			
Interaction energy	−748.9 kJ/mol	−373.0 kJ/mol	
Reaction-field energy	−1,221.8	−985.8	
Total energy	−1,970.7	−1,358.8	
Denatured state			
Interaction energy	−13.8	3.3	
Reaction-field energy	−2,232.3	−1,639.4	
Total energy	−2,246.0	−1,636.2	
ΔE_{EL}	−275.3	−277.3	2.0 kJ/mol

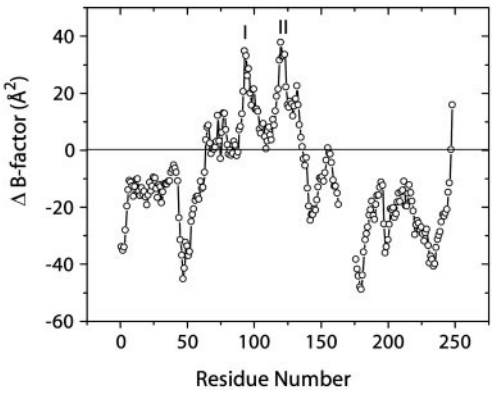

FIG. 8. **Differences in *B*-factors (Å²) averaged for the main-chain atoms *versus* residue number between α-subunits of tryptophan synthases from *P. furiosus* and *S. typhimurium*.** Δ*B*-factor subtracts the values of the *St*-α-subunit from those of the *Pf*-α-subunit. *Peaks I* and *II* correspond to Tyr^{93} and Phe^{120} of the *Pf*-α-subunit, respectively.

DISCUSSION

The α-subunit of tryptophan synthase from the hyperthermophile, *P. furiosus*, was remarkably stable as compared with those from mesophiles, *E. coli* and *S. typhimurium*. Calorimetric results indicated that the higher stability is caused by an entropic effect. This stabilization mechanism was investigated on the basis of structural differences between α-subunits of *P. furiosus* and *S. typhimurium*.

Contribution of the Hydrophobic Interaction—The hydrophobic interaction is one of the important stabilizing forces of folded protein structures (57). The hydrophobic effects have been extensively analyzed by studies with site-directed mutagenesis, and it has been revealed that hydrophobic residues in the interior of a protein contribute to the conformational stability (58–63). Takano *et al.* (64) have found a general rule for the relationship between hydrophobic effect and conformational stability of a protein, using a series of hydrophobic mutants of human lysozyme. Furthermore, the change in unfolding Gibbs energy (ΔG) due to hydrophobic effect between wild-type and mutant proteins ($\Delta\Delta G_{HP}$) could be expressed using changes in accessible surface area (ASA) of nonpolar and polar atoms due to denaturation (65),

$$\Delta\Delta G_{HP} = \alpha\Delta\Delta ASA_{nonpolar} + \beta\Delta\Delta ASA_{polar} \quad \text{(Eq. 6)}$$

where $\Delta\Delta ASA_{nonpolar}$ and $\Delta\Delta ASA_{polar}$ represent the differences in ΔASA of nonpolar and polar atoms of all residues in a protein, respectively, upon denaturation between wild-type and mutant proteins. Using the stability/structure data base for a series of mutant human lysozymes, the parameters, α and β, have been determined to be 0.178 and −0.013 kJ mol^{-1} Å^{-2}, respectively (65). ASA values of proteins in the native state can be calculated using x-ray crystal structures, and those in the denatured state using their extended structures. For the calculation of ASA, C/S atoms in residues were assigned to $ASA_{nonpolar}$ and N/O to ASA_{polar}.

We tried to estimate the difference in contribution of the hydrophobic interaction between *Pf*- and *St*-α-subunits ($\Delta\Delta G_{HP}$). ASA values using x-ray crystal structures of the *Pf*- and *St*-α-subunits in the native state were calculated using the procedure of Connolly (55). The ASA values in the denatured states were calculated from their extended structures of both proteins, which were generated from the native structures using Insight II. As shown in Table IV, the ΔG values due to hydrophobic interaction (ΔG_{HP}) of the *Pf*-α-subunit was lower than that of *St*-α-subunit: the $\Delta\Delta G_{HP}$ value was −79.8 kJ/mol. This means that the higher stability of the *Pf*-α-subunit is not caused by the hydrophobic interaction. This fact could be speculated from the comparison of the contents of hydrophobic residues (Table I): the percent content of hydrophobic residues for the *Pf*-α-subunit (53.6%) was lower than that for the *St*-α-

subunit (58.65%). Makhatadze and Privalov (66) have reported that protein folding is an enthalpically driven process caused by van der Waals interactions between nonpolar groups in the interior of a protein. In the case of the *Pf*-α-subunit, the higher stability was not caused by enthalpic effects, suggesting that the hydrophobic interactions due to nonpolar groups in the interior of the protein do not dominate as compared with those of the *St*-α-subunit. This is also confirmed by the result that the ΔC_p value of the *Pf*-α-subunit (0.52 J K^{-1} g^{-1}) was lower than that for the *St*-α-subunit (0.64 J K^{-1} g^{-1}).

The ratio of hydrophobic residues (Val, Leu, and Ile) is generally higher in hyperthermophile proteins than in mesophile ones (67). But it is not certain that hydrophobic interactions are strengthened at higher temperatures. Thermodynamic analysis of hydrophobic interactions (66) indicates that at high temperature the entropy of hydration of a nonpolar group decreases to zero and the Gibbs energy of the hydrophobic interaction becomes completely enthalpic. This results in the Gibbs energy of the hydrophobic interactions reaching its maximum strength around 75 °C, which is lower than the optimum growth temperatures of hyperthermophiles. This suggests that the hydrophobic interaction does not always act efficiently for the stabilization of a protein at extremely high temperatures over 100 °C.

Contribution of Ion Pairs (Salt Bridge)—It seems that ion pairs (salt bridges) have important roles in protein stability, because they occur frequently in hyperthermophile proteins. However, Xiao and Honig (23) have reported that the roles of individual ion pairs and ion pair networks are variable, and among them some enhance protein stability, whereas others reduce it. The contribution depends strongly on the detailed environment of a particular network. Recently, using computation of ionic interaction energies by solving the Poisson equation in a continuum solvent medium, the ion pairs of glutamate dehydrogenase from *P. furiosus* have been reported to be highly important whereas those in the mesophilic homologs are only marginally stabilizing (13). These reports suggest the necessity to evaluate the strength of each ion pair in a protein. Therefore, we calculated electrostatic free energies in the *Pf*-α-subunit and the *St*-α-subunit solving the Poisson equations numerically for their continuum.

As shown in Table IV, the electrostatic free energy in the native state contributed by the direct interactions among ionic charges was much less in the *Pf*-α-subunit than that in the *St*-α-subunit. Because the *Pf*-α-subunit has more ionizable residues than the *St*-α-subunit, the reaction field energy in the native state of the *Pf*-α-subunit was also much less than that of the *St*-α-subunit. Thus, the ion pairs of the *Pf*-α-subunit greatly contribute to the conformational stability in the native state, as compared with those of the *St*-α-subunit.

However, the stability of the protein should be accounted for by the difference between the native state and the denatured state. Suppose that almost all the protein atoms in the denatured states are well exposed to the solvent molecules with the extended peptide chain conformations. The reaction field energy should become a very large negative value as the number of the ionizable residues increases. Namely, the *Pf*-α-subunit in the denatured state was also more stable than the *St*-α-subunit in the denatured state due to the reaction field energy. Consequently, as shown in the *right-hand column* of Table IV, $\Delta\Delta E$ between ΔE in the *Pf*-α-subunit and that in the *St*-α-subunit is only 2 kJ/mol, which may not explain all of the causes for the difference in the conformational stabilities of the two proteins.

In this continuum model, both absolute free energy values in the native states and in the denatured states were so large that even a slight deviation in the parameters associated with the model would give a large error without revising the parameter values. In the current computation, it is not the comparison between the wild-type protein and the point mutants as once calculated by Kumar *et al.* (13) who neglected the electrostatic free energies in the denatured states. But it is the comparison between proteins from different species with very many substitutions of amino acid residues, and so the electrostatics in the denatured state cannot be neglected.

Recently, Takano *et al.* (24) have estimated the strength of an ionic interaction using a series of ion pair mutants of human lysozyme. Each contribution is not equivalent, but they have found that the contribution correlates linearly with the solvent-inaccessibility of the ion pairs; the contribution of ion pairs is small when 100% accessible, whereas it is about 9 kJ/mol if 100% inaccessible. Then, using accessibility of ion pair atoms in Table III, the contribution due to electrostatic interactions of the *Pf*-α-subunit and the *St*-α-subunit was calculated to be 80.4 and 37.7 kJ mol^{-1}, respectively (ΔG_{EL} in Table IV). This suggests that ion pairs in the *Pf*-α-subunit play an important role in conformational stability.

Contribution of the Entropic Effect—One way of increasing the stability of a protein ($\Delta G = \Delta H - T\Delta S$) is to lower its denaturation entropy (ΔS). The substitutions of other residues by less flexible residues, Pro or Gly (68–70), and the introduction of a disulfide bond (71) are confirmed to increase the stability of proteins. The conformational entropy of a protein in the denatured state can be also lowered by shortening the polypeptide chain. For thermophile proteins, a shortening of the N and C termini and the reduction of loop sizes have been observed (10, 28, 72, 73).

In the case of the *Pf*-α-subunit, 12 residues in the N-terminal, six in the C-terminal, and one residue each in two loops are deleted compared with the sequence of the *St*-α-subunit (Fig. 5). Oobatake and Ooi (74) have estimated the difference in thermodynamic parameters of each amino acid residue upon denaturation. Using these parameters the difference in contribution due to conformational entropy upon denaturation ($-T\Delta S$) between both proteins was calculated to be 51.2 kJ mol^{-1} and 57.2 kJ mol^{-1}, at 25 and 60 °C, respectively (ΔG_{ENT} in Table IV). A great negative value of difference in enthalpy between both proteins ($\Delta\Delta H = -330.2$ kJ mol^{-1} at 60 °C from Fig. 2) could be partly compensated for by the difference in entropic effect (57.2 kJ mol^{-1}). This indicates that the entropic effect due to these deletions plays an important role in the stabilization of the *Pf*-α-subunit. Recently, by analyzing many homologous relationships among many translated open reading frames of DNA from the 20 proteomes, Thompson and Eisenberg (75) have reported that there is a general trend in nature for thermophile sequences to be shorter than their mesophile homologs. This finding has not yet received as much attention as have ion pair networks (75). Present experimental results strongly support this transproteomic evidence.

The N-terminal segments of most prokaryotic tryptophan synthase α-subunits are approximately the same length and contain a helix 0. However, α-subunits from thermophiles, *Bacillus stearothermophilus* and *Thermotoga maritime,* appear to lack eight and 16 residues, respectively, at their N termini, similar to deletion of 12 residues in the *Pf*-α-subunit. These deletions might be related to the higher stability due to entropic effect.

Conclusion—The *Pf*-α-subunit from hyperthermophile, *P. furiosus,* was especially stable in the high temperature region as compared with homologous counterparts from mesophiles. DSC experiments indicated that its higher stability was caused by entropic factors. The tertiary structure of the *Pf*-α-subunit could be analyzed to interpret these thermodynamic character-

istics showing thermostabilization of the hyperthermophile protein. On the basis of structural information of the *Pf*-α-subunit and the *St*-α-subunit, it could be concluded that 1) the contribution of hydrophobic interaction of *Pf*-α-subunit to stability was considerably lower than that of the *St*-α-subunit, and 2) the higher stability of the *Pf*-α-subunit was caused by a decrease in cavity volume in the interior of the molecule, increase in ionic interaction (salt bridge), and entropic effects due to shortening of the polypeptide chain.

Acknowledgments—We greatly thank Prof. Tomitake Tsukihara (Institute for Protein Research, Osaka University) for valuable discussion on the x-ray analysis of the α-subunit structure of tryptophan synthase from *P. furiosus*.

REFERENCES

1. Miles, E. W. (1995) *Subcell. Biochem.* **24,** pp. 207–254
2. Hyde, C. C., Ahmed, S. A., Paduardo, E. A., Miles, E. W., and Davies, D. R. (1988) *J. Biol. Chem.* **263,** 17857–17871
3. Schultz, G. E., and Creighton, T. E. (1969) *Euro. J. Biochem.* **10,** 195–197
4. Day, M. W., Hsu, B. T., Joshua-Tor, L., Park, J.-B., Zhou, Z. H., Adams, M. W. W., and Rees, D. C. (1992) *Protein Sci.* **1,** 1494–1507
5. Chan, M. K., Mukund, S., Kletzin, A., Adams, M. W. W., and Rees, D. C. (1995) *Science* **267,** 1463–1469
6. Hennig, M., Darimont, B., Sterner, R., Kirschner, K., and Jansonius, J. N. (1995) *Structure* **3,** 1295–1306
7. Yip, K. S., Stillman, T. J., Britton, K. L., Artymiuk, P. J., Baker, P. J., Sedelnikova, S. E., Engel, P. C., Pasquo, A., Chiaraluce, R., Conslvi, V., Scandurra, R., and Rice, D. W. (1995) *Structure* **2,** 1147–1158
8. Dedecker, B. S., O'Brien, R., Fleming, P. J., Geider, J. H., Jackson, S. P., and Sigler, P. B. (1996) *J. Mol. Biol.* **264,** 1072–1084
9. Knapp, S., de Vos, W. M., Rice, D., and Ladenstein, R. (1997) *J. Mol. Biol.* **267,** 916–932
10. Tahirov, H., Oki, H., Tsukihara, T., Ogasahara, K., Yutani, K., Ogata, K., Izu, Y., Tsunasawa, S., and Kato, I. (1998) *J. Mol. Biol.* **284,** 101–124
11. Russell, R. J. M., Ferguson, J. M. C., Hough, D. W., Danson, M. J., and Taylor, G. L. (1997) *Biochemistry* **36,** 9983–9994
12. Isupov, M. N., Fleming, T. M., Dalby, A. R., Crowhurst, G. S., Bourne, P. C., and Littlechild, J. A. (1999) *J. Mol. Biol.* **291,** 651–660
13. Kumar, S., Ma, B., Tsai, C.-J., and Nussionv, R. (2000) *Proteins* **38,** 368–383
14. Horovitz, A., Serrano, L., Avron, B., Bycroft, M., and Fersht, A. R. (1990) *J. Mol. Biol.* **216,** 1031–1044
15. Serrano, L., Horovitz, A., Avron, B., Bycroft, M., and Fersht, A. R. (1990) *Biochemistry* **29,** 9343–9352
16. Erwin, C. R., Barnett, B. L., Oliver, J. D., and Sullivan, J. F. (1990) *Protein Eng.* **4,** 87–97
17. Sali, D., Bycroft, M., and Fersht, A. R. (1991) *J. Mol. Biol.* **220,** 779–788
18. Dao-pin, S., Sauer, U., Nicholson, H., and Matthews, B. W. (1991) *Biochemistry* **30,** 7142–7153
19. Lyu, P. C., Gans, P. J., and Kallenbach, N. R. (1992) *J. Mol. Biol.* **223,** 343–350
20. Vetriani, C., Maeder, D. L., Tolliaday, N., Yip, K. S., Stillman, T. J., Britton, K. L., Rice, D. W., Klump, H. H., and Robb, F. (1998) *Proc. Natl. Acad. Sci. U. S. A.* **95,** 12300–12305
21. Spek, E. J., Bui, A. H., Lu, M., and Kallenbach, N. R. (1998) *Protein Sci.* **7,** 2431–2437
22. Sanz-Aparicio, J., Hermoso, J. A., Martinez-Ripoll, M., Gonzalez, B., Lopez-Camacho, C., and Polaina, J. (1998) *Proteins Struct. Funct. Genet.* **33,** 567–576
23. Xiao, L., and Honig, B. (1999) *J. Mol. Biol.* **289,** 1435–1444
24. Takano, K., Tsuchimori, K., Yamagata, Y., and Yutani, K. (2000) *Biochemistry* **39,** 12375–12381
25. Macedo-Riberio, S., Darimont, B., Sterner, R., and Huber, R. (1996) *Structure* **4,** 1291–1301
26. Edmonson, S. P., Qui, L., and Shriver, J. W. (1995) *Biochemistry* **34,** 13289–13304
27. Cavagnero, S., Zhou, Z. H., Adams, M. W., and Chan, S. I. (1995) *Biochemistry* **34,** 9865–9873
28. Starich, M. R., Sandman, K., Reeve, J. N., and Summers, M. (1996) *J. Mol. Biol.* **255,** 187–203
29. Pace, C. N., Shirley, B. A., Mcnutt, M., and Gajiwala, K. (1996) *FASEB. J.* **10,** 75–83
30. Jaenicke, R., and Bohm, G. (1998) *Curr. Opin. Struct. Biol.* **8,** 738–748
31. Merritt, E. A., and Bacon, D. J. (1997) *Methods Enzymol.* **277,** 505–524
32. Sakabe, N. (1991) *Nucl. Instr. Methods Phys. Res.* **A303,** 448–463
33. Otwinowski, Z., and Minor, W. (1997) *Methods Enzymol.* **276,** 307–326
34. Matthews, B. W. (1968) *J. Mol. Biol.* **33,** 491–497
35. Collaborative Computational Project, Number 4. (1994) *Acta Crystallogr. Sect. D Biol. Crystallogr.* **50,** 760–763
36. de La Fortelle, E., and Bricogne, G. (1997) *Methods Enzymol.* **276,** 472–493
37. Abrahams, J. P. (1996) *Acta Crystallogr. Sect. D Biol. Crystallogr.* **52,** 30–42
38. Jones, T. A., Zou, J. Y., Cowan, S. W., and Kjeldgaard, M. (1991) *Acta Crystallogr. Sect. A* **47,** 110–119
39. Brunger, A. T. (1993) *X-plor Version 3.8.5.1* Yale University Press, New Haven, CT
40. Brunger, A. T., Adams, P. D., Clore, G. M., DeLano, W. L., Gros, P., Grosse-Kunstleve, R. W., Jiang, J.-S., Kuszewski, J., Nilges, M., Pannu, N. S., Read, R. J., Rice, L. M., Simonson, T. & Warren, G. L. (1998) *Acta Cryst.* **D54,** 905–921
41. Laskowski, R. A., McArthur, M. W., Moss, D. S., and Thornton, J. M. (1993) *J. Appl. Cryst.* **26,** 283–291
42. Nakamura, H. (1996) *Rev. Biophys.* **29,** 1–90
43. Levitt, M. (1976) *J. Mol. Biol.* **104,** 59–107
44. Sugisaki, Y., Ogasahara, K., Miles, E. W., and Yutani, K. (1990) *Thermochimica Acta* **163,** 117–122
45. Privalov, P. L., and Khechinashvili, N. N. (1974) *J. Mol. Biol.* **86,** 665–684
46. Jaenicke, R., Schurig, H., Beaucamp, N., and Ostendorp, R.,. (1996) *Adv. Protein Chem.* **48,** 181–270
47. Navaza, J. (1994) *Acta Crystallogr. Sect. D Biol. Crystallogr.* **50,** 157–163
48. Banner, D. W., Bloomer, A. C., Petsko, G. A., Philips, D. C., and Wilson, I. A. (1976) *Biochem. Biophys. Res. Commun.* **72,** 146–155
49. Kabsch, W., and Sander, C. (1983) *Biopolymers* **22,** 2577–2637
50. Rhee, S. Parris, K. D., Hyde, C. C., Ahmed, S. A., Miles, E. W., and Davies, D. R. (1997) *Biochemistry* **36,** 7664–7680
51. Weyand, M., and Schlichting, I. (1999) *Biochemistry* **38,** 16469–16480
52. Schneider, T. R., Gerhardt, E., Lee, M., Liang, P. H., Anderson, K. S., and Schlichting, I. (1998) *Biochemistry* **37,** 5394–5406
53. Hiraga, K., and Yutani, K.,. (1997) *J. Biol. Chem.* **272,** 4935–4940
54. Barlow, D. J., and Thornton, J. M. (1983) *J. Mol. Biol.* **168,** 867–885
55. Connolly, M. L. (1993) *J. Mol. Graphics* **11,** 139–141
56. Eriksson, A. E., Baase, W. A., Zhang, X.-J., Heinz, D. W., Blaber, M., Baldwin, E. P., and Matthews, B. W. (1992) *Science* **225,** 178–183
57. Kauzman, W. (1959) *Adv. Protein Chem.* **14,** 1–63
58. Yutani, K., Ogasahara, K. Sugino, Y., and Matsusiro, A. (1977) *Nature* **267,** 274–275
59. Yutani, K., Ogasahara, K., Tsujita, T., and Sugino, Y. (1987) *Proc. Natl. Acad. Sci. U. S. A.* **84,** 4441–4444
60. Kellis, J. T., Nyberg, K., Sali, D., and Fersht, A. R. (1988) *Nature* **333,** 784–786
61. Matsumura, M., Becktel, W. J., and Matthews, B. W. (1988) *Nature* **334,** 406–410
62. Shortle, D., Stites, W. E., and Meeker, A. K. (1990) *Biochemistry* **30,** 9686–9697
63. Sandberg, W. S., and Terwilliger, T. C. (1991) *Proc. Natl. Acad. Sci. U. S. A.* **88,** 1706–1710
64. Takano, K., Yamagata, Y., and Yutani, K. (1998) *J. Mol. Biol.* **280,** 749–761
65. Funahashi, J., Takano, K., Yamagata, Y., and Yutani, K. (1999) *Protein Eng.* **12,** 841–850
66. Makhatadze, G. I., and Privalov, P. L. (1995) *Adv. Protein. Chem.* **47,** 307–425
67. Szilagyi, A., and Zavodszky, P. (2000) *Structure* **8,** 493–504
68. Hecht, M., Sturtevant, J., and Sauer, R. (1986) *Proteins* **1,** 43–46
69. Herning, T., Yutani, K., Inada, K., Kuroki, R., Matsushima, M., and Kikuchi, M. (1992) *Biochemistry* **31,** 7077–7085
70. Nicholson, H., Tronrud, D., Becktel, W., Matthews, B. (1992) *Biopolymers* **32,** 1421–1441
71. Matsumura, M., Becktel, W. J., Levitt, M., and Matthews, B. W (1989) *Proc. Natl. Acad. Sci. U. S. A.* **86,** 6562–6566
72. Russell, R. J. M., Hough, D. W., Danson, M. J., and Taylor, G. L. (1994) *Structure* **2,** 1157–1167
73. Usher, K. C., de la Cruz, A. F., Dahlquist, F. W., Swanson, R. V., Simon, M. I., Remington, S. J. (1998) *Protein Sci.* **7,** 403–412
74. Oobatake, M., and Ooi, T. (1993) *Prog. Biophys. Mol. Biol.* **59,** 237–284
75. Thompson, M. J., and Eisenberg, D. (1999) *J. Mol. Biol.* **290,** 594–604
76. Kraulis, P. J. (1991) *J. Appl. Crystallogr.* **24,** 946–950

Entropic Stabilization of the Tryptophan Synthase α-Subunit from a Hyperthermophile, *Pyrococcus furiosus* : X-RAY ANALYSIS AND CALORIMETRY

Yuriko Yamagata, Kyoko Ogasahara, Yusaku Hioki, Soo Jae Lee, Atsushi Nakagawa, Haruki Nakamura, Masami Ishida, Seiki Kuramitsu and Katsuhide Yutani

J. Biol. Chem. 2001, 276:11062-11071.
doi: 10.1074/jbc.M009987200 originally published online December 15, 2000
